COMMUNICATION

Chinese Journal of Structural Chemistry

Atomically Dispersed Main Group Magnesium on Cadmium Sulfide as the Active Site for Promoting Photocatalytic Hydrogen Evolution Catalysis

Ran Chen[1†], Juan Chen[1†], Huinan Che[1], Gang Zhou[1], Yanhui Ao[1*] and Bin Liu[2,3*]

[1]*Key Laboratory of Integrated Regulation and Resource Development on Shallow Lakes, Ministry of Education, College of Environment, Hohai University, Nanjing 210098, China*

[2]*School of Chemical and Biomedical Engineering, Nanyang Technological University, Singapore 637459, Singapore*

[3]*Division of Chemistry and Biological Chemistry, School of Physical and Mathematical Sciences, Nanyang Technological University, 21 Nanyang Link, Singapore 637371, Singapore*

ABSTRACT Photoabsorption charge separation/transfer and surface reaction are the three main factors influencing the efficiency of photocatalysis. Band structure engineering has been extensively applied to improve the light absorption of photocatalysts, however, most of the developed photocatalysts still suffer from low photocatalytic performance due to the limited active site(s) and fast recombination of photogenerated charge carriers. In this work, atomically dispersed main group magnesium (Mg) is introduced onto CdS monodispersed nanospheres, which greatly enhances the photocatalytic hydrogen evolution reaction. The photocatalytic hydrogen evolution reaction rate reaches 30.6 mmol·$g_{catalyst}^{-1}$·h^{-1}, which is about 11.8 and 2.5 times that of pure CdS and Pt (2 wt.%)-CdS. The atomically dispersed Mg on CdS acts as an electron sink to trap photogenerated electrons, and at the same time, greatly reduces the Gibbs free energy of hydrogen evolution reaction (HER) and accelerates HER.

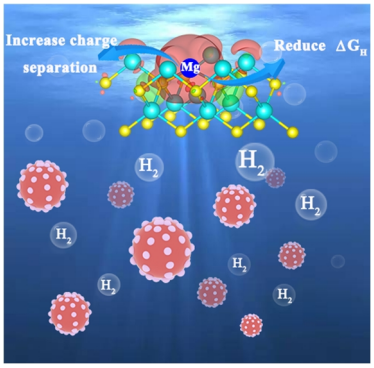

Keywords: CdS, hydrogen, photocatalysis, atomically dispersed, main group metal

n INTRODUNTION

In the long progress of seeking renewable energy to tackle energy crisis and alleviate environmental deterioration, hydrogen shows great potential to replace traditional fossil fuels.[1–5] Photocatalysis provides a green approach to generate renewable hydrogen or hydrogen Peroxide.[6,7] However, practical application of photocatalytic hydrogen production is challenging because of the low energy conversion efficiency.[8–10] Three main factors including photoabsorption, charge carrier separation and surface catalysis determine the overall energy efficiency of a photocatalytic process. While the band structure of photocatalysts has been extensively engineered to enhance light absorption, the fast recombination of photogenerated electrons and holes as well as the lack of effective active site(s) still limit the photocatalytic performance.[11]

Generally, reactive active sites played an important role in photocatalytic process via activating the target compound with lower energy demands.[12] Coupling co-catalysts to expose more active sites onto light absorbing semiconductors delivers impressive performance in photocatalysis.[13–17] Over the past few years, various noble metal, transition metal sulfide, phosphide and carbide co-catalysts have been studied to enhance photocatalytic hydrogen evolution reaction.[18–21] Different from conventional co-catalysts of clusters or nanoparticles, isolated atoms exhibit unique characteristics of well-controlled coordination environment, accelerated charge transfer and close to 100% atom utilization efficiency in catalysis.[22–28]

In this work, we develop atomically dispersed main group Mg atom decorated CdS photocatalysts by a simple hydrothermal method (Figure 1a). The single Mg atoms on CdS not only act as an electron sink to trap photogenerated electrons, enhancing charge separation, but also greatly reduce the Gibbs free energy of HER, which together accelerate catalytic dynamics and boost the efficiency of photocatalytic hydrogen evolution reaction.

n RESULTS AND DISCUSSION

Morphology and Phase Structure. CdS based photocatalysts were synthesized by a hydrothermal reaction (Figure 1a). The morphologies of the as-prepared CdS and single Mg atom decorated CdS ($Mg_xCd_{1-x}S$) photocatalysts were examined in detail. Transmission electron microscope (TEM) images of $Mg_{0.02}Cd_{0.98}S$ (Figure 1b–c and Supplementary Figure 1) exhibit monodispersed nanospheres with a mean diameter of 450 nm. Compared to pure CdS, the morphology of $Mg_{0.02}Cd_{0.98}S$ is well maintained after the introduction of Mg. High-resolution TEM (HR-TEM) images in Figure 1c and d show well-organized lattice with an interplanar spacing of 0.32 nm, which can be assigned to the (101) facets of wurtzite CdS.[29] Magnesium was uniformly distributed in the matrix of CdS (Figure 1e), suggesting that Mg atoms have been successfully incorporated into CdS in the atomically dispersed states.

While extended X-ray absorption fine structure (EXAFS) is not possible to be applied to extract the coordination environment of Mg, DFT calculations were employed to study the structure of $Mg_{0.02}Cd_{0.98}S$. Different configurations of Mg sites on/in CdS were constructed (Supplementary Figure 2), including the replacement Mg sites (site A, B and C) and the interstitial Mg sites

DOI: 10.14102/j.cnki.0254-5861.2021-0027

Chinese Journal of Structural Chemistry

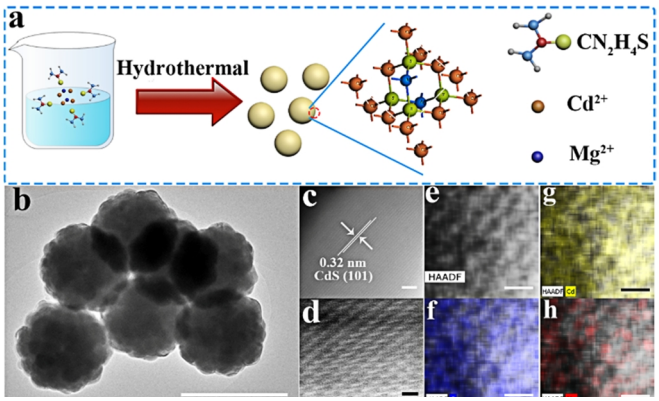

Figure 1. a) Schematic illustration showing the preparation route for $Mg_xCd_{1-x}S$ photocatalyst. b) TEM (scale bar: 500 nm), c–d) HR-TEM (scale bar: c 2 nm and d 0.5 nm), and e–h) HAADF-STEM (scale bar: 0.5 nm) image with elemental mappings.

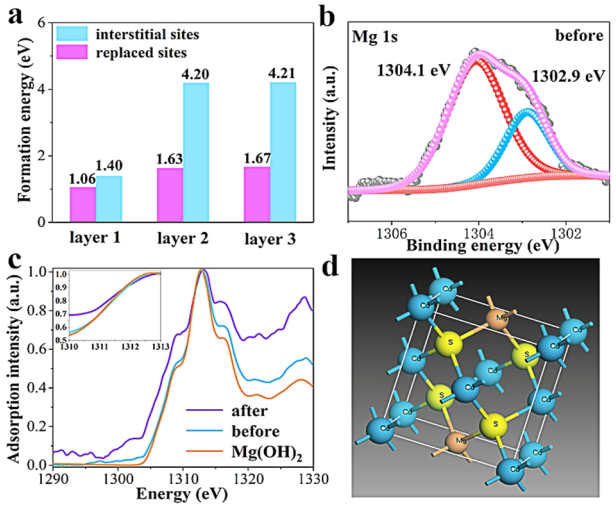

Figure 2. a) Formation energy of $Mg_{0.02}Cd_{0.98}S$ acquired from DFT calculation. b) XPS spectra of Mg 1s. c) Mg K-edge XANES spectra. Inset shows the enlarged spectra. d) Structure model of $Mg_{0.02}Cd_{0.98}S$.

(site D, E and F). Figure 2a compares the formation energy of different Mg sites, suggesting that the incorporation of Mg on the surface of CdS is most favourable. X-ray photoelectron spectroscopy (XPS) was adopted to investigate the valence states of pure CdS and $Mg_{0.02}Cd_{0.98}S$. As displayed in Figure 2b, the Mg 1s XPS spectrum can be deconvoluted into two peaks at ca. 1304.1 and 1302.9 eV. The binding energy at 1304.1 eV belongs to Mg–O,[30] while the lower binding energy at 1302.9 eV originates from Mg–S that was formed by the substitution of Cd.[31] As observed in Supplementary Figure 3a and b, characteristic peaks at ca. 405.3 and 412.1 eV belonging to Cd $3d_{5/2}$ and Cd $3d_{3/2}$ and ca. 161.5 and 162.7 eV corresponding to S $2p_{3/2}$ and S $2p_{1/2}$ can be clearly detected in pure CdS photocatalyst.[32,33] Both Cd 3*d* and S 2*p* XPS spectra shift to lower binding energies after the introduction of Mg with the formation of Mg–S–Cd bond. Furthermore, X-ray diffraction (XRD) and Raman spectroscopy were performed to study the structure of $Mg_{0.02}Cd_{0.98}S$ (Supplementary Figure 4–5), and the results are discussed in the Supplementary Information. To gain more information about the valence state of the Mg atom, X-ray absorption near the edge structure (XANES) was examined as shown in Figure 2c, from which the valence state of Mg in $Mg_{0.02}Cd_{0.98}S$ is determined to be in the range of 0 to +2. Additionally, the edge of Mg XANES spectrum is sensitive to the coordination environment.[34,35] As compared in Figure 2c, the XANES spectrum edge of $Mg_{0.02}Cd_{0.98}S$ is slightly right-shifted as compared to that of the reference $Mg(OH)_2$, suggesting that Mg partially substitutes Cd in the as-prepared $Mg_{0.02}Cd_{0.98}S$ as shown in Figure 2d.

Photocatalytic Performance. The photocatalytic hydrogen evolution reaction under visible light irradiation ($\lambda \geq 420$ nm) over the as-synthesized CdS photocatalysts was evaluated in S^{2-}/SO_3^{2-} (as the hole scavenger) solution. As shown in Figure 3a, pure CdS without loading of any co-catalyst exhibits very poor photocatalytic activity with photocatalytic hydrogen evolution reaction rate of only 2.6 $mmol \cdot h^{-1} \cdot g_{catalyst}^{-1}$. Interestingly, the photocatalytic hydrogen evolution is greatly promoted after introducing Mg into CdS. The optimized photocatalytic hydrogen evolution reaction rate for $Mg_xCd_{1-x}S$ at x = 0.02 reaches 30.6 $mmol \cdot h^{-1} \cdot g_{catalyst}^{-1}$ with quantum efficiency of 40.7% at 420 nm, significantly outperforming the photocatalytic hydrogen evolution reaction rate of Pt (2 wt.%)-CdS (12.1 $mmol \cdot h^{-1} \cdot g_{catalyst}^{-1}$). The introduction of Mg atoms could afford more active sites and the atomically dispersed Mg on CdS acts as an electron sink to trap photogenerated electrons, thus promoting the greatly enhanced photocatalytic hydrogen evolution performance. Further increasing Mg content in $Mg_xCd_{1-x}S$ reduces the photocatalytic activity, possibly due to the formation of deep level recombination centers.[36] The obtained hydrogen evolution reaction results of $Mg_xCd_{1-x}S$ samples are compared with previously reported CdS-based photocatalysts in Table S1. More details about the comparative study over various CdS-based photocatalysts are shown in Supplementary Figure 6–7. Besides activity, the $Mg_xCd_{1-x}S$ photocatalysts also show excellent photocatalytic stability. As shown in Supplementary Figure 8, nearly no deactivation was observed during the five consecutive photocatalytic cycles. Furthermore, the photocatalyst after photocatalytic hydrogen evolution reaction was characterized by XRD, Raman, XPS and TEM (Supplementary Figure 9–11), showing that the photocatalyst could well maintain its morphology and electronic structure during photocatalytic reaction, testifying the excellent durability. Additionally, XANES spectrum of $Mg_{0.02}Cd_{0.98}S$ after photocatalytic hydrogen evolution reaction in Figure 2c shows increased absorption intensity as compared to the as-synthesized $Mg_{0.02}Cd_{0.98}S$, indicating a decreased valence state of Mg after photocatalytic hydrogen evolution reaction. In photocatalytic hydrogen evolution reaction, atomically dispersed Mg atoms may act as an electron sink to trap photogenerated electrons, which causes a partial reduction of Mg to a lower oxidation state.

To understand the significantly improved photocatalytic activity of $Mg_xCd_{1-x}S$, the light absorption property was first studied. As shown in Figure S12, CdS exhibits a UV-vis absorption edge at around 550 nm, corresponding to a bandgap of 2.25 eV.[37] Meanwhile, the absorption edge shows a continuous blue shift with increasing the Mg content in $Mg_xCd_{1-x}S$, indicating that the improved photocatalytic activity of $Mg_xCd_{1-x}S$ should not result from the enhanced light absorption. The charge recombination

DOI: 10.14102/j.cnki.0254-5861.2021-0027

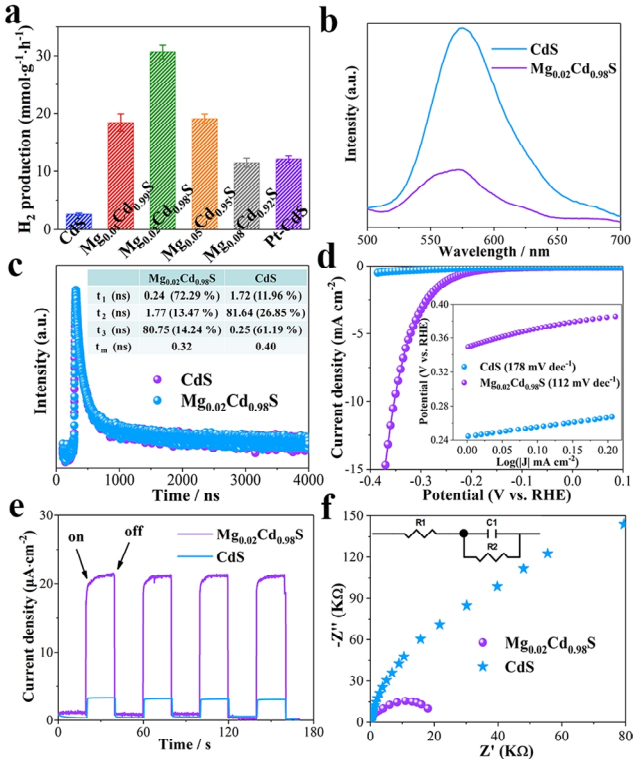

Figure 3. a) Photocatalytic performance of CdS, a series of $Mg_xCd_{1-x}S$ and Pt (2 wt.%)-CdS. b–c) PL and time-resolved PL results. d) Linear sweep voltammetry curves and the corresponding HER Tafel plots. e) Transient photocurrent response. f) Electrochemical impedance spectra.

characteristics were evaluated by photoluminescence (PL). A much-quenched PL emission and shorter fluorescence lifetime were observed on $Mg_{0.02}Cd_{0.98}S$ as compared to that on CdS (Figure 3b and c), suggesting much efficient photogenerated charge carrier separation on $Mg_{0.02}Cd_{0.98}S$. Additionally, the surface catalytic activity of CdS and $Mg_{0.02}Cd_{0.98}S$ was compared as shown in Figure 3d. It is clear to see that $Mg_{0.02}Cd_{0.98}S$ possesses a much higher activity in catalyzing HER, which displays a much larger current density at the same applied potential as compared to CdS. Both improved charge separation and enhanced HER catalysis ensure $Mg_{0.02}Cd_{0.98}S$ with much higher photocurrent (Figure 3e) and reduced charge transfer resistance (Figure 3f). Moreover, from the ultraviolet photoelectron spectroscopy (UPS) results and the corresponding band structures (Supplementary Figure 13–14), the conduction band (CB) edge of $Mg_{0.02}Cd_{0.98}S$ is closer to the Fermi level (E_F) as compared to that of pure CdS, which shall effectively promote carrier density and electron transfer.

To gain further theoretical information on the promoting effect of atomically dispersed Mg on the photocatalytic hydrogen evolution reaction process, density functional theory (DFT) calculations were performed. Figure 4a summarizes the possible Mg sites in $Mg_{0.02}Cd_{0.98}S$. Based on the formation energy calculation of different Mg sites, the atomically dispersed Mg site (site 3) in $Mg_{0.02}Cd_{0.98}S$ is thermodynamically most favourable. As calculated, the differential charge density as displayed in Figure 4b shows that electrons tend to transfer to Mg atoms near the surface of $Mg_{0.02}Cd_{0.98}S$, suggesting that Mg atoms can act as an efficient electron sink to trap photogenerated electrons, matching

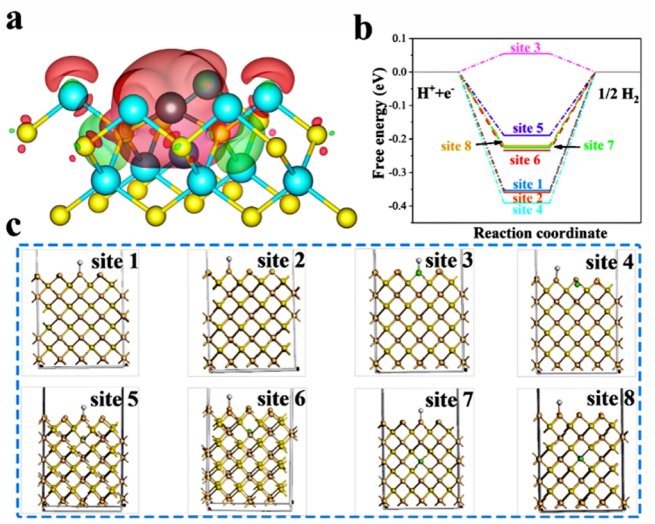

Figure 4. a) Calculated differential charge density for $Mg_{0.02}Cd_{0.98}S$. b) The calculated Gibbs free energy for hydrogen adsorption. c) Atomic structure models showing possible Mg sites in $Mg_{0.02}Cd_{0.98}S$.

well with the experimental observation. Furthermore, the HER Gibbs free energy calculation as displayed in Figure 4c shows that the hydrogen adsorption energy (DG_H) significantly deceases if Mg substitutes Cd in CdS at the surface. With Mg atoms replacing deeper Cd sites, the DG_H increases but is still lower than that for pure CdS, indicating the crucial role of isolated Mg atoms as the active sites in catalyzing HER at the surface of CdS.

n CONCLUSION

In summary, a novel atomically dispersed main group Mg atom on CdS photocatalyst has been successfully developed for photocatalytic hydrogen evolution reaction, which exhibits extraordinary photocatalytic activity and stability. The atomically dispersed Mg on CdS not only acts as an efficient electron sink to trap photogenerated electrons to promote charge separation, but also effectively reduces the Gibbs free energy of HER, which together accelerate catalytic dynamics and boost the efficiency of photocatalytic hydrogen evolution reaction.

n METHODS

Materials Synthesis. All chemicals were of analytical grade and used as received without further purification. $Mg_xCd_{1-x}S$ photocatalysts (x = 0, 0.01, 0.02, 0.05 and 0.08) were synthesized by a simple hydrothermal method. Typically, 0.005 mol of $Cd(CH_3COO)_2{\cdot}2H_2O$ was added into 60 mL of deionized (DI) water with CH_4N_2S under stirring, followed by adding a certain amount of $Mg(NO_3)_2{\cdot}6H_2O$. Next, the above solution was transferred into a 100 mL Teflon-lined stainless-steel autoclave and heated at 160 °C in an electric oven for 24 h. After reaction, the product was washed several times by DI water, harvested by centrifugation and dried at 60 °C overnight. Pt (2 wt.%)-CdS photocatalyst was synthesized under vacuum atmosphere using a photodeposition method. Briefly, 10 mg of the as-prepared CdS was put into 50 mL DI water, followed by adding sacrificial reagent containing 0.35 M Na_2SO_3 and 0.25 M $Na_2S{\cdot}9H_2O$ under stirring. Subsequently, 0.1 mL of 0.04 M $H_2PtCl_6{\cdot}6H_2O$ was added into the above solution. Next, the solution was degassed

DOI: 10.14102/j.cnki.0254-5861.2021-0027

and vacuumed, and illuminated under a 300 W Xenon lamp with a 420 nm cut-off filter for 2 h to load Pt nanoparticles on CdS.

Characterization. X-ray diffraction (XRD) was employed to analyze the catalyst structure using a Rigaku/SmartLab diffractometer system with CuKα radiation (λ = 1.5418 Å). The morphology of the catalyst was examined by scanning electron microscopy (SEM, Hitachi S4800), transmission electron microscopy (TEM) and high-angle annular dark-field scanning transmission electron microscopy (HAADF-STEM). UV-vis diffuse reflectance spectra (DRS) were collected on a Shimadzu/UV-3600 equipment. Photoluminescence (PL) was performed on a Hitachi/F-7000 apparatus to examine the charge separation characteristics. The exponential fitting formula is listed as follows:

$$R(t) = B_1 e^{(\frac{-t}{t_1})} + B_2 e^{(\frac{-t}{t_2})} + B_3 e^{(\frac{-t}{t_3})}$$

X-ray photoelectron spectra (XPS) were carried out on PHI 5000 Versaprobe with Al-Kα radiation. Ultraviolet photoelectron spectroscopy (UPS) was conducted on ESCALAB 250Xi. Raman spectroscopy was performed on a LabRRM HR Evolution. Soft X-ray absorption spectroscopy (XAS) spectra at the Mg K-edge were collected at the NSRRC TLS BL20A1 station in Taiwan, China.

Electrochemical Measurements. All of the electrochemical tests were performed on a Chenhua CHI660D electrochemical workstation in a standard three-electrode configuration with a Ag/AgCl electrode as the reference electrode, a graphite rod as the counter electrode and a catalyst coated glassy carbon electrode as the working electrode. All measured potentials vs. Ag/AgCl were converted to the potentials vs. reversible hydrogen electrode (RHE) by the Nernst equation: $E_{RHE} = E_{Ag/AgCl} + 0.059 \times pH + 0.198$.

Photocatalytic H_2 Evolution Measurements. Photocatalytic performance of the as-prepared photocatalysts was examined in a 150 mL quartz reactor under visible light illumination. Typically, 5 mg of the photocatalyst was added into 50 mL solution, containing 0.25 M Na_2S and 0.35 M Na_2SO_3 as the sacrificial reagent. Then, the system was vacuumed and illuminated under a Xenon lamp with a 420 nm cut-off filter (CELHXF300, Beijing China Education Au-light Co., Ltd). The H_2 produced was quantified by an online gas chromatography (GC 7900) equipped with a TCD detector. The apparent quantum efficiency (AQE) was calculated using the following equation:

$$AQE = \frac{\text{Number of reacted electrons}}{\text{Number of incident photons}} \times 100\%$$

$$= \frac{2 \times \text{Number of evolved } H_2 \text{ molecules}}{\text{Number of incident photons}} \times 100\%$$

Theoretical Calculation. DFT calculation was performed using plane-wave basis Vienna ab initio simulation package code with generalized gradient approximation. The cutoff energy for expanding Kohn-Sham wave functions was chosen to be 460 eV and the vacuum space of 20 Å was used to avoid the interaction between periodical images. The Monkhorst-Pack k-points grid was 8 × 8 × 1 and all forces on the free ions were 0.03 eV/Å. The activation energies were calculated using the climbing nudged elastic band method. Electromagnetic simulations were obtained by a FEM. Differential charge density was calculated according to previous work.[38]

n ACKNOWLEDGEMENTS

We are grateful for the financial support from the Natural Science Foundation of China (51979081), Fundamental Research Funds for the Central Universities (No. B200202103), Ministry of Education of Singapore (Tier 1: RG4/20 and Tier 2: MOET2EP10120-0002), Agency for Science, Technology and Research (AME IRG: A20E5c0080), and PAPD.

n AUTHOR INFORMATION

Corresponding authors. E-mails: andyao@hhu.edu.cn (Y. Ao) and liubin@ntu.edu.sg (B. Liu).

n COMPETING INTERESTS

Ran Chen and Juan Chen contributed equally to this work.
The authors declare no competing interests.

n ADDITIONAL INFORMATION

Supplementary information is available for this paper at http://manu30.magtech.com.cn/jghx/EN/10.14102/j.cnki.0254-5861.2021-0027

For submission: https://mc03.manuscriptcentral.com/cjsc

n REFERENCES

(1) Wang, J. F.; Chen, J.; Wang, P. F.; Hou, J.; Wang, C.; Ao, Y. H. Robust photocatalytic hydrogen evolution over amorphous ruthenium phosphide quantum dots modified g-C_3N_4 nanosheet. *Appl. Catal. B-Environ.* **2018**, 239, 578–585.

(2) Lin, H. X.; Chen, C. P.; Zhou, T. H.; Zhang, J. Two-dimensional covalent-organic frameworks for photocatalysis: the critical roles of building block and linkage. *Solar RRL* **2020**, 5, 2000458.

(3) Ouyang, T.; Wang, X. T.; Mai, X. Q.; Chen, A. N.; Tang, Z. Y.; Liu, Z. Q. Coupling magnetic single-crystal $Co_2Mo_3O_8$ with ultrathin nitrogen-rich carbon layer for oxygen evolution reaction. *Angew. Chem. Int. Ed.* **2020**, 9, 11948–11957.

(4) Mu, R. H.; Ao, Y. H.; Wu, T. F.; Wang, C.; Wang, P. F. Synergistic effect of molybdenum nitride nanoparticles and nitrogen-doped carbon on enhanced photocatalytic hydrogen evolution performance of CdS nanorods. *J. Alloy. Compd.* **2020**, 812, 151990.

(5) Jiang, X. H.; Zhang, L. S.; Liu, H. Y.; Wu, D. S.; Wu, F. Y.; Tian, L.; Liu, L. L; Zou, J. P.; Luo, S. L.; Chen, B. B. Silver single atom in carbon nitride catalyst for highly efficient photocatalytic hydrogen evolution. *Angew. Chem. Int. Ed.* **2020**, 59, 23112–23116.

(6) Wang, J. F.; Wang, P. F.; Wang, C.; Ao, Y. H. In-situ synthesis of well dispersed CoP nanoparticles modified CdS nanorods composite with boosted performance for photocatalytic hydrogen evolution. *Int. J. Hydrogen Energ.* **2018**, 43, 14934–14943.

(7) Che, H. N.; Gao, X.; Chen, J.; Hou, J.; Ao, Y. H.; Wang, P. F. Iodide-induced fragmentation of polymerized hydrophilic carbon nitride for high-performance quasi-homogeneous photocatalytic H_2O_2 production. *Angew. Chem. Int. Ed.* **2020**, 60, 25546–25550.

(8) Liu, X.; Zhao, Y. X.; Yang, X. F.; Liu, Q. Q.; Yu, X. H.; Li, Y. Y.; Tang, H.; Zhang, T. R. Porous Ni_5P_4 as a promising cocatalyst for boosting the photocatalytic hydrogen evolution reaction performance. *Appl. Catal. B: Environ.* **2020**, 275, 119144.

(9) Liu, M. R.; Hong, Q. L.; Li, Q. H.; Du, Y. H.; Zhang, H. X.; Chen, S. M.; Zhou, T. H.; Zhang, J. Cobalt boron imidazolate framework derived

DOI: 10.14102/j.cnki.0254-5861.2021-0027

cobalt nanoparticles encapsulated in B/N codoped nanocarbon as efficient bifunctional electrocatalysts for overall water splitting. *Adv. Funct. Mater.* **2018**, 28, 1801136.

(10) Zhou, S. Q.; Wang, Y.; Zhou, K.; Ba, D. Y.; Ao, Y. H.; Wang, P. F. In-situ construction of Z-scheme g-C_3N_4/WO_3 composite with enhanced visible-light responsive performance for nitenpyram degradation. *Chin. Chem. Lett*. **2021**, 32, 2179–2182.

(11) Yang, M. Q.; Han, C.; Xu, Y. J. Insight into the effect of highly dispersed MoS_2 versus layer-structured MoS_2 on the photocorrosion and photoactivity of CdS in graphene-CdS-MoS_2 composites. *J. Phys. Chem. C* **2015**, 119, 27234–27246.

(12) Shi, R.; Ye, H. F.; Liang, F.; Wang, Z.; Li, K.; Weng, Y. X.; Lin, Z. S.; Fu, W. F.; Che, C. M.; Chen, Y. Interstitial P-doped CdS with long-lived photogenerated electrons for photocatalytic water splitting without sacrificial agents. *Adv. Mater.* **2018**, 1705941.

(13) Li, W.; Lee, J. R.; Jackel, F. Simultaneous optimization of colloidal stability and interfacial charge transfer efficiency in photocatalytic Pt/CdS nanocrystals. *ACS Appl. Mater. Interfaces* **2016**, 8, 29434–29441.

(14) Wang, J. F.; Wang, P. F.; Hou, J.; Qian, J.; Wang, C.; Ao, Y. H. In situ surface engineering of ultrafine Ni_2P nanoparticles on cadmium sulfide for robust hydrogen evolution. *Catal. Sci. Technol.* **2018**, 8, 5406–5415.

(15) Yin, X. L.; He, G. Y.; Sun, B.; Jiang, W. J.; Xue, D. J.; Xia, A. D.; Wan, L. J.; Hu, J. S. Rational design and electron transfer kinetics of MoS_2/CdS nanodots-on-nanorods for efficient visible-light-driven hydrogen generation. *Nano Energy* **2016**, 28, 319–329.

(16) Ma, X. W.; Lin, H. F.; Li, Y. Y.; Wang, L.; Pu, X. P.; Yi, X. J. Dramatically enhanced visible-light-responsive H_2 evolution of $Cd_{1-x}Zn_xS$ via the synergistic effect of Ni_2P and 1T/2H MoS_2 cocatalysts. *Chin. J. Struct. Chem.* **2021**, 40, 7–22.

(17) Li, M. X.; Guan, R. Q.; Li, J. X.; Zhao, Z.; Zhang, J. K.; Dong, C. C.; Qi, Y. F.; Zhai, H. J. Performance and mechanism research of Au-HSTiO_2 on photocatalytic hydrogen production. *Chin. J. Struct. Chem.* **2020**, 39, 1437–1443.

(18) Ran, J. R.; Gao, G. P.; Li, F. T.; Ma, T. Y.; Du, A. J.; Qiao, S. Z. Ti_3C_2 MXene co-catalyst on metal sulfide photo-absorbers for enhanced visible-light photocatalytic hydrogen production. *Nat. Commun.* **2017**, 8, 1–10.

(19) Ran, J. R.; Zhang, J.; Yu, J. G.; Jaroniec, M.; Qiao, S. Z. Earth-abundant cocatalysts for semiconductor-based photocatalytic water splitting. *Chem. Soc. Rev.* **2014**, 43, 7787–7812.

(20) Yao, X. X.; Hu, X. L.; Cui, Y. Y.; Huang, J. L.; Zhang, W. J.; Wang, X. H.; Wang, D. W. Effect of Mie resonance on photocatalytic hydrogen evolution over dye-sensitized hollow C-TiO_2 nanoshells under visible light irradiation. *Chin. Chem. Lett.* **2021**, 32, 1135–1138.

(21) Bi, W. T.; Li, X. G.; Zhang, L.; Jin, T.; Zhang, L. D.; Zhang, Q.; Luo, Y.; Wu, C. Z.; Xie, Y. Molecular co-catalyst accelerating hole transfer for enhanced photocatalytic H_2 evolution. *Nat. Commun.* **2015**, 6, 8647.

(22) Yu, F.; Wang, L. C.; Xing, Q. J.; Wang, D. K.; Jiang, X. H.; Li, G. C.; Zheng, A. M.; Ai, F. R.; Zoua, J. P. Functional groups to modify g-C_3N_4 for improved photocatalytic activity of hydrogen evolution from water splitting. *Chin. Chem. Lett.* **2020**, 31, 1648–1653.

(23) Zhang, H. B.; Wang, Y.; Zuo, S. W.; Zhou, W.; Zhang, J.; Lou, X. W. D. Isolated cobalt centers on $W_{18}O_{49}$ nanowires perform as a reaction switch for efficient CO_2 photoreduction. *J. Am. Chem. Soc.* **2021**, 143, 2173–2177.

(24) Cheng, N. C.; Stambula, S.; Wang, D.; Banis, M. N.; Liu, J.; Riese, A.; Xiao, B. W.; Li, R. Y.; Sham, T. K.; Liu, L. M. Platinum single-atom and cluster catalysis of the hydrogen evolution reaction. *Nat. Commun.* **2016**, 7, 13638.

(25) Liu, L. C.; Corma, A. Metal catalysts for heterogeneous catalysis: from single atoms to nanoclusters and nanoparticles. *Chem. Rev.* **2018**, 118, 4981–5079.

(26) Lai, W. H.; Miao, Z. C.; Wang, Y. X.; Wang, J. Z.; Chou, S. L. Atomic-local environments of single-atom catalysts: synthesis, electronic structure, and activity. *Adv. Energy Mater.* **2019**, 9, 1900722.

(27) Ding, S. P.; Hulsey, M. J.; Perez-Ramirez, J.; Yang, N. Transforming energy with single-atom catalysts. *Joule* **2019**, 3, 2897–2929.

(28) Liu, L. C.; Corma, A. Metal catalysts for heterogeneous catalysis: from single atoms to nanoclusters and nanoparticles. *Chem. Rev.* **2018**, 118, 4981–5079.

(29) Zhu, B. J.; Qiu, K. P.; Shang, C. X.; Guo, Z. X. Naturally derived porous carbon with selective metal-and/or nitrogen-doping for efficient CO_2 capture and oxygen reduction. *J. Mater. Chem. A* **2015,** 3, 5212–5222.

(30) Mahajan, R.; Prakash, R.; Kumar, S.; Kumar, V.; Choudhary, R. J.; Phase, D. M. Surface and luminescent properties of $Mg_3(PO_4)_2$:Dy^{3+} phosphors. *Optik* **2021**, 225, 165717.

(31) Du, C. L.; Zhu, Y. Q.; Wang, Z. T.; Wang, L. Q.; Younas, W.; Ma, X. L.; Cao, C. B. Cuprous self-doping regulated mesoporous CuS nanotube cathode materials for rechargeable magnesium batteries. *ACS Appl. Mater. Interfaces* **2020**, 12, 35035–35042.

(32) Yuan, Y. J.; Chen, D. Q.; Yang, S. H.; Yang, L. X.; Wang, J. J.; Cao, D. P.; Tu, W. G.; Yu, Z. T.; Zou, Z. G. Constructing noble-metal-free Z-scheme photocatalytic overall water splitting systems using MoS_2 nanosheets modified CdS as a H_2 evolution photocatalyst. *J. Mater. Chem. A* **2013**, 5, 21205–21213.

(33) Kumar, D. P.; Hong, S.; Reddy, D. A.; Kim, T. K. Ultrathin MoS_2 layers anchored exfoliated reduced graphene oxide nanosheet hybrid as a highly efficient cocatalyst for CdS nanorods towards enhanced photocatalytic hydrogen production. *Appl. Catal. B-Environ.* **2017**, 212, 7–14.

(34) Ildefonse, P.; Calas, G.; Flank, A. M.; Lagarde, P. Low Z elements (Mg, Al, and Si) K-edge X-ray absorption spectroscopy in minerals and disordered systems. *Nucl. Instrum. Methods Phys. Res. Sect. B: Beam Interact. Mater. At.* **1995**, 97, 172–175.

(35) Yoshimura, T.; Tamenori, Y.; Iwasaki, N.; Hasegawa, H.; Suzuki, A.; Kawahata, H. Magnesium K-edge XANES spectroscopy of geological standards. *J. Synchrotron Radiat.* **2013**, 20, 734–740.

(36) Li, S.; Zhang, L. J.; Jiang, T. F.; Chen, L. P.; Lin, Y. H.; Wang, D. J.; Xie, T. F. Construction of shallow surface states through light Ni doping for high-efficiency photocatalytic hydrogen production of CdS nanocrystals. *Chem. Eur. J.* **2014**, 20, 311–316.

(37) Huang, Q. Z.; Tao, Z. J.; Ye, L. Q.; Yao, H. C.; Li, Z. J. $Mn_{0.2}Cd_{0.8}S$ nanowires modified by CoP_3 nanoparticles for highly efficient photocatalytic H_2 evolution under visible light irradiation. *Appl. Catal. B-Environ.* **2018**, 237, 689–698.

(38) Zhou, G.; Hu, Y. Y.; Long, L. Y.; Wang, P. F.; Shan, Y.; Wang, L. L.; Guo, J. H.; Zhang, C. G.; Zhang, Y. M.; Liu, L. Z. Charged excited state induced by ultrathin nanotip drives highly efficient hydrogen evolution. *Appl. Catal. B-Environ.* **2020**, 262, 118305.

Received: November 5, 2021
Accepted: December 1, 2021
Published: January 13, 2022

DOI: 10.14102/j.cnki.0254-5861.2021-0027